www.czasopisma.pan.pl PAN POLSKA AKADEMIA NAUK www.journals.pan.pl

A R C H I V E S O F M E T A L L U R G Y A N D M A T E R I A L S

Volume 59 2014 Issue 4

DOI: 10.2478/amm-2014-0243

G.Y. PEREZ-MEDINA*, H.F. LOPEZ**, F.A. REYES-VALDÉS*, A. GARZA-GOMEZ*, LUIS M. LÓPEZ-OCHOA***

WELDING EFFECTS ON THE MECHANICAL INTEGRITY OF A TRIP800 STEEL: A COMPARISON OF LASER CO_2 AND GMAW PROCESSES

WPŁYW SPAWANIA NA INTEGRALNOŚĆ MECHANICZNĄ STALI TRIP800: PORÓWNANIE SPAWANIA LASEROWEGO ZE SPAWANIEM ELEKTRODĄ TOPLIWĄ

In this work a strip of a transformation induced plasticity (TRIP) steel was welded using gas metal arc welding (GMAW) and Laser CO_2 welding (LBW) processes and the resultant strength and ductility of the welded joints evaluated. It was found that LBW lead to relatively high hardness in the fusion zone, FZ where the resultant microstructure was predominantly martensite. The relative volume fractions of phases developed in the welded regions were quantitatively measured using color metallography combined with X-ray diffraction analyses. It was found that the heat affected zone, HAZ developed the maximum amount of martensite (up to 32%) in the steel welded using LBW besides a mixture of bainite, retained austenite and ferrite phases. In contrast, a relatively low percent of martensite (10.8%) was found in the HAZ when the GMAW process was implemented.

Keywords: Laser, gmaw, retained austenite, color metallography

Pas ze stali typu TRIP poddano spawaniu elektrodą topliwą oraz spawaniu laserowemu i oceniono wytrzymałość i plastyczność uzyskanych połączeń spawanych. Stwierdzono, że spawanie laserowe prowadzi do uzyskania stosunkowo wysokiej twardości w strefie łączenia, gdzie powstałą mikrostrukturę stanowi głównie martenzyt. Względne udziały objętościowe faz w spawanych obszarach zmierzono ilościowo za pomocą barwnej metalografii w połączeniu z dyfrakcyjną analizą rentgenowską. Stwierdzono, że w przypadku stali spawanej laserowo strefa wpływu ciepła zawiera najwięcej martenzytu (do 32%), a oprócz tego mieszaninę bainitu, resztkowego austenitu i ferrytu. Natomiast w strefie wpływu ciepła uzyskanej podczas spawania elektrodą topliwą stwierdzono stosunkowo niską zawartość martenzytu (10,8%).

1. Introduction

The design of fuel efficient vehicles coupled with the need for high impact strength has lead to the development of engineering materials with outstanding toughness. In turn, advanced high strength steels (AHSS) have been developed that allow the manufacture of low weight car bodies using thin sheet gauge of less than 1 mm [1, 2]. Among the AHSS considered for applications in the automotive sector are transformation induced plasticity (TRIP) steels [1-3]. TRIP steels possess predominantly ferrite/bainite phase mixtures with significant amounts of retained austenite. These steels exhibit relatively high work hardenabilites and remarkable formability. The enhanced plastic behavior is attributed to a strain induced transformation of the retained austenite into martensite during plastic straining [2, 3]. It is well known that the amount of retained austenite and hence the TRIP effect is strongly influenced by the carbon content [4] and strain temperatures [3]. At low carbon levels, the amount of retained austenite is relatively low and it transforms almost immediately upon reaching yielding. At increasing carbon contents, the amount and stability of the retained austenite, both increase and it transforms at elevated levels of plastic straining such as the ones that occur during a sudden crash event [3, 5].

The use of relatively thin TRIP steel sheet in the manufacture of car bodies requires of homogeneous mechanical properties in addition to a relatively high corrosion resistance. Accordingly, a reduction of thickness and/or microstructural changes due to welding/joining effects can be detrimental for the mechanical integrity of these steels. Thus, it is important to establish the effect of welding processes and parameters on the resultant microstructures and on the exhibited mechanical properties including corrosion resistance.

Among the main concerns related to welding is the formation of unwanted martensite [6, 7]. It has been found that in low heat input welding processes such as laser beam welding (LBW), high carbon martensites can form that lead to embrittlement [6, 7]. However, there are few reports on the effects of laser beam welding on the resultant microstructures and on the weld mechanical integrity. Accordingly, in this work the

* CORPORACIÓN MEXICANA DE INVESTIGACIÓN EN MATERIALES CALLE CIENCIA Y TECNOLOGÍA #790, FRACC. SALTILLO 400, SALTILLO, COAH. MÉXICO

** MATERIALS DEPARTMENT, UNIVERSITY OF WISCONSIN-MILWAUKEE, 3200 N. CRAMER STREET, MILWAUKEE WI 53201, USA

*** UNIVERSIDAD DE LA RIOJA. ESCUELA TÉCNICA SUPERIOR DE INGENIERÍA INDUSTRIAL. APPLIED THERMODYNAMICS AND ENERGY GROUP OF RESEARCH. LA PAZ STREET 93, 26 LOGROÑO. LA RIOJA. SPAIN

TABLE 1

Chemical composition of the AHSS TRIP 800

Wt%	C	Mn	Si	P	Al	Cu	Cr	Ni	Mo	Sn
TRIP800	0.232	1.653	1.55	0.010	0.041	0.033	0.033	0.036	0.018	0.006
FM Wire	0.09	1.55	0.35	0.010	0.10	0.25	0.50	2.10	0.35	--

effect of welding on the exhibited microstructures and on the strength of a TRIP steel was investigated using a low and a high heat input welding process. For this purpose, a gas metal arc welding (GMAW) and a Laser CO_2 welding processes were employed in welding a TRIP thin sheet steel currently used in the automotive sector.

2. Experimental

The TRIP800 steel was supplied by the Italian Institute of Welding as 1.6 mm steel sheet. Tab I gives the chemical composition of the TRIP steel and the filler metal wire used in the GMAW process. From the steel sheet, tensile bars were cut with dimensions 244×70×1.6 mm and welded by GMAW and Laser CO_2 processes. Tab II shows the exhibited mechanical properties of the TRIP 800 steel in the as-received condition. The welding parameters used in the GMAW and Laser CO_2 processes are given in Tab III. In the case of the GMAW, the filler metal was of the ER110S-G type (see Tab I) with a 1.6 mm diameter suitable for 780 MPa high tensile strength steels. The welding equipment employed was a Robot COMAU, CG4, RCC1, 17900582. In laser welding the equipment used was a CO_2-LBW-unit, EL.EN-RTM of 6 kW with 6 degrees of freedom.

TABLE 2

Mechanical properties of the AHSS TRIP 800

Base Metal	Yield Strength [MPa]	Ultimate Tensile Strength [MPa]	Elongation [%]
TRIP800	450	800	28

TABLE 3

Welding Parameters using GMAW and CO_2 laser processes in a TRIP800 steel

Welding Process	Joint type	Current [A]	Voltage [V]	Power [kW]	Welding speed [mm/min]	Heat Input [J/mm]
GMAW	Butt Joint	136	13	--	799.84	132.6
Laser CO_2	Butt Joint	--	--	4,5	3699.76	72.97

The exhibited microstructures and fracture modes of the Welded TRIP steels were characterized by metallographic means including optical, scanning electron microscopy (SEM) including EDX, as well transmission electron microscopy (TEM). The thin-foil samples used for TEM examinations were prepared by mechanical thinning of the welded steel down to a thickness of approximately 50nm with a double beam equipment (SEM/FIB). The amount of retained austenite developed in the WM and HAZ was determined using X-ray diffraction means. The etchant solution used was Klemm's I (1 g K2S2O5 potassium metabisulfite, 79.4 g Na2S2O3-5H2O Sodium Thiosulfate) to reveal the structure of the HAZ and WM. Lepera (1% aqueous sodium metabisulfite with 4% Picral) was used to reveal the BM structure and 2% Nital followed by heat tinting, to reveal ferrite grain boundaries and any cementite as described by Vander Voort and Amar, [8, 9]. The exhibited hardness of the various welding regions was determined by Vickers micro-hardness profile determinations. In addition, the tensile strength and ductility of the as-received steel, as well as the welded strips was determined using a universal testing machine. In this work, no formability no crash tests were performed as the work was focused on the microstructural characterization of the failure and of the failure regions.

3. Results and Discussion

Welded Microstructures

Metallographic determinations followed methods for identification and characterization of phases in TRIP steels [8, 9]. Accordingly, the exhibited microstructural features of the TRIP steel in the as-received condition are shown in Fig. 1a. Notice the mixture of ferrite and bainite including retained austenite. In addition, some martensite packets were found as shown in Fig. 1a. The resultant microstructures in the WM and HAZ of the TRIP800 steel welded using LBW are shown in Figs. 1b and 1c, respectively. No carbide phases or inclusions were found in any of the welded regions of either laser of GMAW welded samples. Quantitative determinations (see Fig. 2a) indicate that the amount of martensite present in the BM using LBW is relatively small (7%). In contrast, the martensite content in the WM region was approximately 24%. Moreover, martensite levels exceeding 30% were present in the HAZ. In particular, the zone adjacent to the HAZ-BM regions were characterized by the presence of martensite on the HAZ side while phase coarsening occurred on the BM side (see Fig. 3). Further evidence of phase coarsening was provided by SEM observations of this region. Notice from these micrographs the presence of relatively coarse acicular ferrite (Fig. 4a) in a predominantly bainitic matrix and phase refinement away from the HAZ-BM interface (Fig, 4b). In order to further disclose the relative locations and amounts of the various phases, TEM observations (see Figs. 5a-c) were carried out on the HAZ, FZ and BM. Notice the presence of elongated bainite strips in the FZ separated by films of retained austenite at the interfaces, in agreement with the literature [10].

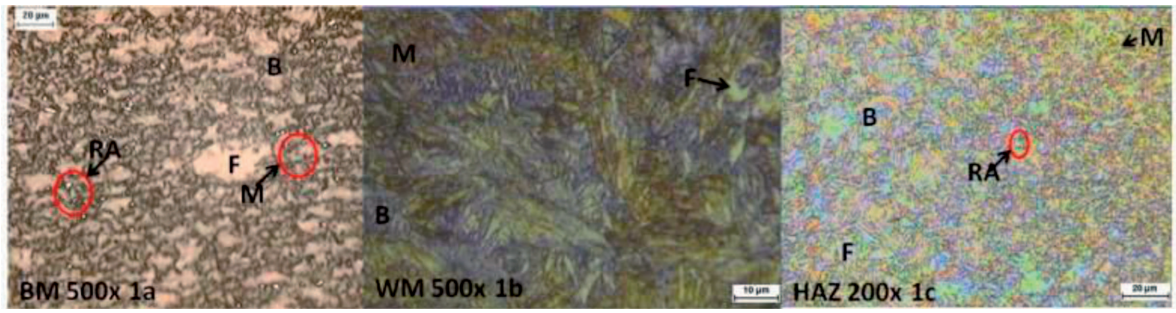

Fig. 1. LBW microstructures of the AHSS TRIP800 in (a) BM, (b) WM and (c) HAZ

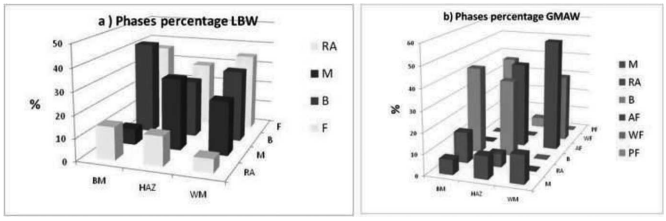

Fig. 2. Phase percentage in (a) LBW, (b) GMAW

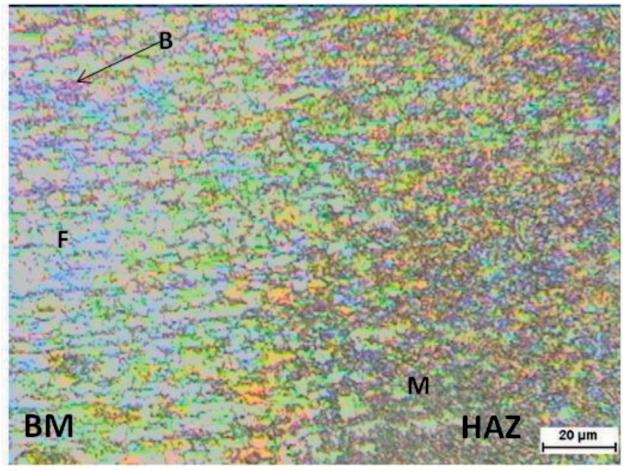

Fig. 3. Optical micrograph showing existing contrast between the HAZ and the adjacent BM due to the relatively large amounts of martensite in the HAZ

In addition, high carbon plate martensite packets were found in both, the HAZ and BM regions (Figs. 5b-c). Hence, it is evident that the exhibited weld microstructures are strongly influenced by the steel composition (i e preferentially C, Mn and Si contents), as well as by the thermal cycles experienced in the various weld regions.

A determination of the relative volume percents of the various phases was possible by quantitative metallography using color tint etching [8, 9] (see Fig. 4a). Moreover, the relative amounts of RA in the BM, FZ and HAZ were also determined using X-ray diffraction (XRD) (Fig. 4b) and Cu Kα radiation and by considering the expression [4].

$$V\gamma = \frac{1.4I_\gamma}{I_\alpha + 1.4I_\gamma} \tag{1}$$

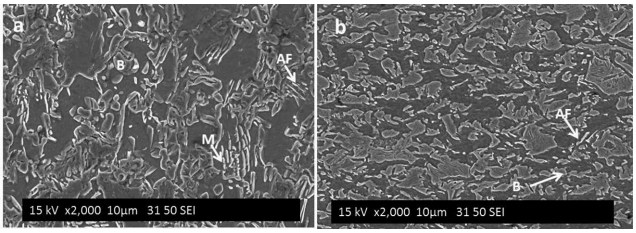

Fig. 4. Acicular ferrite and martensite in (a) the adjacent HAZ-BM regions and (b) phase refinement away from the HAZ zone

Where Iγ is the average intensity of the austenite peaks and Iα is the highest intensity of the ferrite peak. The XRD results are given in Tab III. Notice from this table that the % RA in the HAZ and FZ drops down to 11.29% when compared with 12.54% RA in the BM. From these resuts, it is evident that the relatively fast cooling rates exhibited in the FZ and

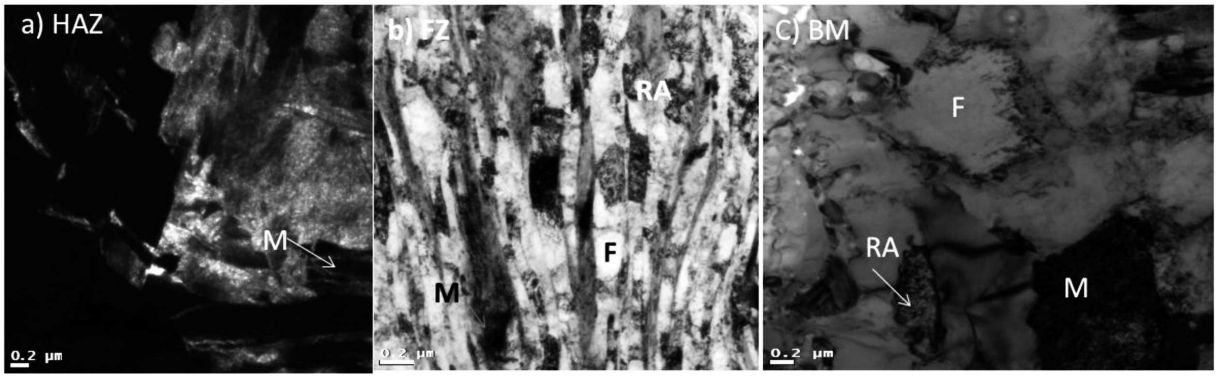

Fig. 5. Bright field TEM micrographs of (a) heat affected zone, (b) fusion zone and (C) base metal showing location and morphology of martensite, M, ferrite, F and retained austenite, RA

HAZ favored the austenite to martensite transformation reducing the amounts of RA. Under these conditions it is likely that there is not enough time to promote austenite stabilization through carbon enrichment and/or Mn partition in the austenite phase. In the case of Mn, its partition can be rather limited due to its relatively low diffusivity.

Similar phase determinations were made in samples welded using the GMAW process. Fig. 6a-b shows the resultant microstructures in the WM and HAZ regions. Notice that the exhibited microstructures are mixtures of martensite, ferrite (Allotriomorphic, Widmanstatten and Polygonal) and retained austenite. Quantitative determinations of the relative amounts are shown in Fig. 2b. In particular, it is found that there is a significant amount of martensite in the WM region (13.5%). Yet, the relative amounts of martensite developed in the HAZ are relatively small (10.8%). In turn, this suggests that GMAW is highly effective in minimizing martensite formation in the HAZ.

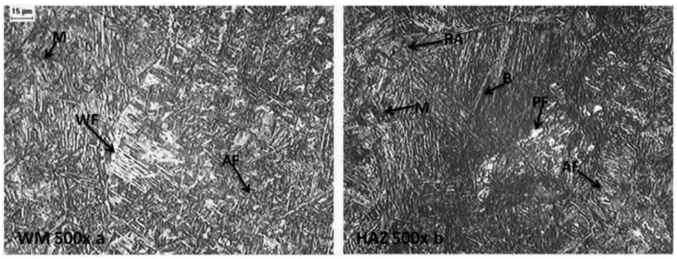

Fig. 6. GMAW microstructure of (a) the WM and (b) HAZ

An estimation of the cooling rates exhibited by the weld metal can be made using the expression [3]:

$$\frac{\partial\theta}{\partial t} = -\frac{2\pi K_s^2}{\alpha}\left(\frac{v\Delta x}{Q}\right)^2 (\theta - \theta_0)^3 \qquad (2)$$

Where θ is the welding temperature (K), t time in seconds, k_s is the thermal conductivity of the steel, α is the thermal diffusivity in m^2/s, v is the welding speed (m/s), Q is the power input and θ_o is the room temperature (K). From these estimations, cooling rates of the order of 144.67^o K/s are estimated for GMAW and of 417.81^o K/s for Laser CO_2 welding. From these results, it is clear that laser welding gives rise to relatively fast cooling rates. In addition, critical cooling rates for the transformation of austenite (γ) to martensite can be determined from continuous cooling transformation (CCT) diagrams. Unfortunately there are no reports on the continuous cooling transformation (CCT) curves for the TRIP800 steel.

Li et al [11] and Bhadeshia et al [12], have proposed thermodynamically and kinetically based models for predicting CCT diagrams in a wide range of steels [12]. From these estimations, it is found that in the present steel, critical cooling rates for the formation of martensite are between 45 and 90°C/s. Moreover, from the work of Gould et al [13], martensitic structures in the weld regions are likely to form at cooling rates above 90°C/sec in TRIP800 steels. In addition, alloying additions such as Mn an austenite stabilizer greatly improve hardenability and this can lead to a reduction in critical cooling rates for the formation of martensite to values of 10-100°C/s, which are well below the expected cooling rates in GMAW. Thus, embrittlement in the WM regions can be a potential problem, particularly when Laser CO_2 welding is employed as the carbon content of the steel is relatively high (0.23% C).

Since the heat input during welding using the GMAW process is almost twice the heat input of the laser process (see Tab III), the exhibited cooling rates are significantly reduced in this case. However, a dominant martensitic structure is still developed in the WM regions as evidenced by the microhardness "top hat" profiles (see Fig. 7a). Nevertheless, the steel used as filler metal contains relatively low carbon (0.09) suggesting that the martensite developed in the WM region is a low carbon martensite which does not harm the mechanical properties of the weld. Moreover, the Si content of the filler metal is relatively low (0.2-0.55%) to avoid cementite formation and thus promote retained austenite [14].

Microhardness

Figs. 7a-b show the microhardness profiles for the various regions of the welded TRIP800 using the two welding processes. The numbers represent the locations of indentations at 1 mm spacings. Notice that in the laser welded TRIP800 steel the average microhardness increases from 275 HV in the BM to up to 500 HV in the HAZ and over 600 HV in the WM regions. In particular, the microhardness profiles resemble a "top hat" morphology [8] with a maximum hardness of 600 HV in the parting line. These microhardness profiles are attributed to the development of athermal martensite [13] which is no longer a function of the cooling rates. In the GMAW, similar microhardness profiles are exhibited in the WM nugget indicating the development of athermal martensite. In this case, maximum Vickers hardness values of up to 500 HV were found in the welded regions.

From the microhardness measurements it is evident that welding leads to a significant increase in hardness in the welded regions in both welding processes. In turn, both welding processes promote martensite development in the WM zones. Also, martensite development in the HAZ all the way to the adjacent BM regions is favored by the LBW process as evidenced by the relatively high hardness (points 4 and 11 in Fig. 7a). This effect was not observed when GMAW was employed.

In the LBW process the lack of embrittlement at the parting line of the WM due to martensite formation can be attributed to the transformed amounts of martensite which do not seem to reach a critical volume fraction, as well as to the type of martensite. In low carbon martensites, the dominant structure is lath martensite with relatively large dislocation densities and no detrimental effects on the exhibited steel toughness [15]. In the case of the GMAW process, lath martensites are likely to form as the filler metal composition is rather low in carbon (0.09% C, see Tab. 1).

In contrast, high carbon twinned martensites can develop in the WM regions when the LBW is implemented. This is strongly dependant on the cooling cycle and the chemistry of the steel including any carbon dilution effects from the adjacent BM region. At high cooling rates, the steel transforms from austenite under non-equilibrium conditions. Under these conditions, there is very little time for ferrite formation in the intercritical temperature regions. Whenever, ferrite formation occurs, carbon is rejected to neighboring γ grains. In turn, carbon enrichment of the γ phase can take place leading to

high carbon martensites in agreement the work of G. R. Speich [16] on the presence of high carbon twinned martensites in a TRIP steel in the as-received condition. In turn, plausible embrittlement due to martensite occurrence is highly dependent on the amount and type of martensite and hence on the steel hardenability.

Weld Strength

Tab IV show the tensile strength (UTS) and ductility exhibited by the welded TRIP800 steels. Although, the number of tensile tests was limited, notice from this table that both, UTS and % elongation drop in the laser welded strips when compared with the GMAW ones. In the laser welded specimens the maximum UTS values did not reach 800 MPa in contrast with the ones welded using GMAW. Also, the elongation of the laser welded TRIP steels drops down to 15% or below when compared with the elongation of GMAW which are of the order of 24%. In turn, this clearly indicates that laser welding of TRIP800 steels can lead to a reduction in the steel strength when compared with the GMAW process.

TABLE 4
Tensile test results of TRIP800 Welded by laser CO_2 and GMAW processes

Process	No, Sample	% Elongation	UTS Mpa.	Fracture Zone
Laser CO2	1	15.00	748.43	BM adjacent HAZ
	2	21.67	789.83	BM
	3	15.00	767.37	BM adjacent HAZ
GMAW	4	24.17	837.07	BM
	5	23.33	842.14	BM
	6	21.67	838.68	BM

Confirmation for the loss of strength and ductility was found by examining the fracture regions (see Fig. 8). It was found that in the specimens welded using GMAW the fracture location was always in the BM regions away from the welded regions. The fracture surfaces were typical of a ductile material with numerous dimples and appreciable plastic deformation (see Fig. 8a). In turn this indicated that the mechanical strength of the GMAW welded regions was superior or equal to the strength of the BM. In contrast, in the laser welded steels, fracture occurred in the BM regions adjacent to the HAZ as shown in Fig. 8b. Also, the fracture appearance was cleavage with what seemed to be chevron markings (see Figs. 9a-b). Notice the lack of enough ductility as the fracture surfaces were relatively flat and there was a lack of appreciable cavitation typical of ductile rupture.

As mentioned before in this work, in LBW the HAZ develops appreciable martensite volume fractions beyond the amounts found in the WM regions (see Fig. 2). Moreover, the BM region adjacent to the HAZ the microstructure is made up coarse ferrite-bainite constituents and possible retained austenite. Hence, during tensile testing this region becomes susceptible to fracture as the martensite in the adjacent HAZ fractures in a brittle fashion (see Figs. 8-9). Also, the high hardness profiles (Fig. 7a) in the BM region adjacent to the HAZ can be accounted for through either the development of internal stresses associated with the transformation and/or the formation of strain induced martensite from any retained austenite. This effect is not observed in the GMAW process and it can be attributed to the lack of appreciable martensite in the HAZ regions.

Finally, the loss of strength and ductility in the steel due to LBW stems from the development of appreciable martensite in the HAZ neighboring the BM. This effect could not be linked to the presence of unwanted martensite in the WM region. Laser welding is known to give rise to minimal microstructural damage as the WM and HAZ are relatively narrow. Hence, the outcome of this work indicates that the potential for martensite embrittlement might occur at the HAZ/BM boundaries. Apparently, the loss of mechanical strength can be attributed to the development of martensite coupled with coarsening of the ferrite/bainite microstructure on the BM side. Hence, additional work is needed to identify LBW parameters which will avoid the loss of strength and ductility at these regions.

4. Conclusions

Microhardness measurements were combined with tensile testing in investigating the weldability of a TRIP 800 steel sheet using GMAW and LBW processes. It was found that:

1. Welding using LBW and GMAW lead to the development of relatively high contents of martensite (>20%).
2. In the LBW process, the highest amounts of martensite were found in the HAZ.
3. GMAW promoted the development of mixtures of predominantly bainite and acicular ferrite phases in the HAZ.
4. The measured mechanical properties indicated that in samples welded using LBW, the BM region adjacent to the HAZ underwent brittle fracture in the form of cleavage.
5. In both welding processes, no embrittlement could be found in the WM regions that can be attributed to the formation of martensite.

Acknowledgements

Thanks for financial support from Consejo Estatal de Ciencia y Tecnología from the state of Coahuila in Mexico.

REFERENCES

[1] N. Kapustka, C. Conrardy, S. Babu, Effect of GMAW process and Material Conditions on DP 780 and TRIP 780 Welds, Welding Journal 2008.
[2] L. Laquerbe, J. Neutjens, Ph. Harlet, F. Caroff, and P. Cantinieaux, 41 st. MWSP Conf. Proceeds. ISS **37**, 89-99 (1999).
[3] Y. Sakuma, D.K. Matlock, and G. Krauss, Metall. Trans. A **23A**, 1221-1232 (1992).
[4] M. De Meyer, D. Vanderschueren, and B.C. De Cooman, 41 st. MWSP Conf. Proceeds. ISS **37**, 265-276 (1999).
[5] I.D. Choi et al., Deformation behaviour of low carbon TRIP sheet steels at high strain rates. ISIJ Int **42** (12), 1483-9 (2002).

[6] J.E. Gould, L.R. Lehman, S. Holmes, A design of experiments evaluation of factors affecting the resistance spot weldability of high-strength steels. Proc. Sheet Metal Welding Conference VII, AWS Detroit Section (1996).
[7] J.E. Gould, D. Workman, Fracture morphologies of resistance spot welds exhibiting hold time sensitivity behavior. Proc. Sheet Metal Welding Conference VIII, AWS Detroit Section (1998).
[8] K. De Amar, J.G. Speer, D.K. Matlock, Color Tint-Etching for Multiphase Steels. Advanced materials and processes 2003.
[9] George Vander Voort, Using microstructural analysis to solve practical problems, welding Metallography-Ferrous Metals 2004.
[10] J. Chen, K. Sand, M.S. Xia, C. Ophus, R. Mohammadi, M.L. Kuntz, Y. Zhou, and D. Mitlin, TEM and nanoindentation Study of Weld Zone Microstructure of Diode Laser Joined. Metals and Materials Society and ASM International 2008.
[11] M.V. Li, D.V. Niebuhr, L.L. Meekisho, and D.G. Atteridge, A computational model for the prediction of steel hardenability. Metallurgical and Materials Transactions **29B** (6), 661-672 (1998).
[12] H.K.D.H. Bhadeshia, and L.-E. Svensson, Mathematical Modeling of Weld Phenomena, eds, H. Cerjack and K. E. Easterling, Institute of Metals, London, 109-180 (1993).
[13] J.E. Gould, S.P. Khurana, T. Li, Predictions of microstructures when welding automotive advanced high-strength steels; Welding Journal, AWS, May 2006, 111 (2006).
[14] J. Speer, D.K. Matlock, B.C. De Cooman, J.G. Schroth, Carbon partitioning into austenite after martensite transformation; Science Direct, January 2003.
[15] George Vander Voort, Martensite and retained austenite, Industrial Heating, April 2009.
[16] G.R. Speich, Metall. Trans. A **3**, 1972.

Received: 20 December 2013.